Thermal and Morphological Characterization of Binary Blends of Fractions of 1-Octene LLDPE

F. DEFOOR,[1] G. GROENINCKX,[1,*] H. REYNAERS,[1] P. SCHOUTERDEN,[2] and B. VAN DER HEIJDEN[2]

[1]Katholieke Universiteit Leuven, Departement Scheikunde, Laboratorium voor Macromoleculaire Structuurchemie, Celestijnenlaan 200 F, B 3001 Heverlee, Belgium; [2]DOW BENELUX N.V., P.O. Box 48, 4530 AA Terneuzen, The Netherlands

SYNOPSIS

An ethylene/1-octene linear low-density polyethylene (LLDPE B) has been fractionated with respect to the short-chain branching content of the molecules, using the preparative temperature-rising elution fractionation (PTREF) technique. The LLDPE B studied, which is characterized by a high degree of heterogeneity on the level of the molecular weight and the comonomer content, was fractionated into six fractions having a more homogeneous intermolecular comonomer distribution. As a result of the differences in the chain microstructure of the fractions, a strong change in the thermal characteristics such as onset temperature of crystallization from the melt and melting temperature has been found. The morphology of the fractions, i.e., spherulitic texture and semicrystalline lamellar ordering, also strongly depends on the chain microstructure. In an attempt to elucidate the mutual influence of molecules having a different chain microstructure, as occurring within the unfractionated copolymer, blends of preparative TREF fractions were prepared and investigated with respect to their thermal behavior and morphology. © 1993 John Wiley & Sons, Inc.

INTRODUCTION

Linear low-density polyethylene (LLDPE) is known to have a very heterogeneous chain microstructure with respect to the molecular weight and the short-chain branching distribution.[1-3] Fractionation of LLDPE with regard to the molecular weight[4] or branching content[1,4-7] is a straightforward method to obtain insight into the very complex crystallization and melting[8] behavior as well as into the morphology.[9,10] Studies on high-density polyethylene (HDPE) demonstrated the dependence of the lamellar morphology[11-15] and the spherulitic texture[12,16] on the molecular weight. In the case of low-density polyethylene (LDPE), the presence of long- and short-chain branches is the principal factor determining the morphology.[17] Although the molecular weight is certainly also of importance for LLDPE,[1,4] the amount and type of comonomer and the inter- and intramolecular distribution of the comonomer are the dominant factors for the spherulitic texture[5,18] and the lamellar morphology[9,10,18,19] and as a consequence for the melting behavior as well.

Recent studies on binary blends of HDPE with LDPE and LLDPE have shown that cocrystallization of the components depends on the difference in their chain microstructure.[20-25] Blending of HDPE with LLDPE can give interesting information on the influence of the linear molecules with respect to the morphology. However, the composition of these blends is even more complex compared to that of plain LLDPE.

In this paper, a 1-octene LLDPE (LLDPE B) has been fractionated with respect to the short-chain branching content of the molecules. The spherulitic texture and the lamellar morphology of these fractions and their thermal behavior were investigated as a function of the branching content. Blends have been prepared using the fractions with the highest and the lowest branching contents. Since both fractions originate from the same LLDPE sample, the blends can yield valuable information on their mu-

* To whom correspondence should be addressed.

Journal of Applied Polymer Science, Vol. 47, 1839–1848 (1993)
 CCC 0021-8995/93/101839-10

tual influence with respect to the crystallization behavior and morphology in the unfractionated LLDPE sample.

EXPERIMENTAL

Materials

A commercial ethylene/1-octene LLDPE copolymer (LLDPE B) prepared in a solution process has been used. The characteristics of the unfractionated LLDPE B are summarized in Table I.

Fractionation Method

The incorporation of 1-octene into the polyethylene chain leads to the formation of short-chain branches (hexyl groups), resulting in a decrease of the crystallizability of the polymer chain. Preparative temperature-rising elution fractionation (PTREF) has been used to fractionate the LLDPE B with respect to the short-chain branching content; this method is based on the differences in chain crystallizability.[26,27] The fractionation consists mainly of two steps: a slow and controlled crystallization of the copolymer from a dilute solution during cooling and the subsequent separation into different fractions upon elution during an increase of the elution temperature. A complete description of the PTREF technique has been given elsewhere.[7] During the preparative fractionation of LLDPE B, six fractions (B0–B5) were obtained at elution temperatures of 25, 55, 70, 80, 95, and 120°C, respectively. The amount of material obtained for fraction B0 was too small to be considered for further complete investigation.

Characterization Techniques

The average value for the short-chain branching content of the fractions has been determined with IR spectrophotometry by measuring the intensity of the methyl absorbtion band at 1378 cm^{-1}. A correction has to be made for absorption of the methylene groups at 1368 and 1352 cm^{-1}. A high-temperature GPC has been used to determine the molecular weight distribution of the fractions. The temperature of the column and injector was 140°C during the measurements; 1,2,4-trichlorobenzene was used as solvent.

Melting endotherms and crystallization exotherms were recorded using a Perkin-Elmer Delta Series DSC-7. The cooling and heating rates were 5°C per minute. All the fractions and blends were held at 150°C in the melt during 10 min before measuring the crystallization exotherms. The samples were stored at room temperature during 1 week before measuring the melting endotherms. As a result of isothermal crystallization at room temperature, some fractions exhibit a small melting peak at 40°C. The presence of this melting peak makes it possible to detect the onset of the melting in a more accurate way. The degree of crystallinity χ_c was calculated by integration of the melting peak area and taking the enthalpy of fusion of 100% crystalline polyethylene as 293 J/g.

A small-angle laser light-scattering (SALLS) device (consisting of a He/Ne laser beam, a Mettler FP-82 hot stage as sample holder, and a CCD camera as detector connected to an image analysis system) was used to determine the crystallization kinetics of the samples and to determine the spherulitic morphology during crystallization from the melt.

SAXS measurements were performed using a rotating anode generator operating at 50 kV and 150 mA, combined with a Kratky slit collimation system, and recorded on films. The periodicity L of the fractions and the blends was calculated by application of Bragg's law to the peak maximum of the desmeared and Lorentz-corrected scattered intensity. The one-dimensional correlation function[28] $\gamma_1(r)$

Table I Characteristics of LLDPE B

SCB[a]	12.9
$\bar{M}_w$	97,500
$\bar{M}_w/\bar{M}_n$	4.83
Density ρ (g/cm^3)	0.917

[a] Average short-chain branching content: number of methyl groups per 1000 carbon atoms.

Table II Elution Temperature (T_{el}), Average Short-Chain Branching Content (SCB), Weight-Average Molecular Weight ($\bar{M}_w$), and Polydispersity of the Fractions

Sample	T_{el}	SCB	$\bar{M}_w$	$\bar{M}_w/\bar{M}_n$
LLDPE B	—	12.9	97,500	4.83
B5	120	3	194,000	2.76
B4	95	7	123,500	3.85
B3	80	15	76,500	3.32
B2	70	22	62,000	3.39
B1	55	33	35,000	3.64
B0	25	43	20,000	4.16

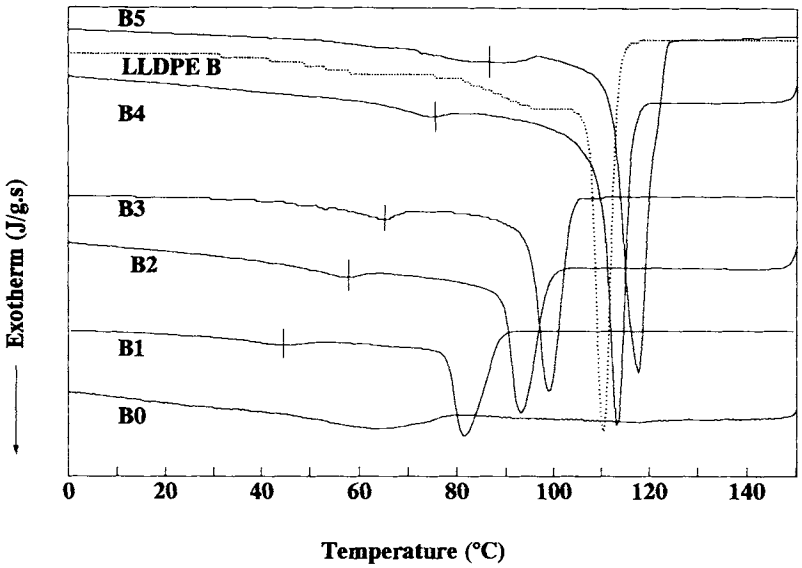

Figure 1 Crystallization exotherms of the fractions and LLDPE B.

was calculated to obtain information about the extent and perfection of the lamellar stacking.

Blend Preparation

Three different blend compositions of the fractions B1 and B5 (having the highest and the lowest branching content, respectively) were prepared. The blends will be referred to their composition in weight percent B5/B1, as 80/20, 50/50, and 20/80. The blends were prepared by dissolution of the fractions B1 and B5 in *p*-xylene at 125°C, followed by precipitation in cold acetone as the nonsolvent. The blends were then dried in a vacuum oven at 50°C during 3 days to remove all the solvent traces.

RESULTS AND DISCUSSION

Chain Microstructure

Table II gives the average SCB content, the weight-average molecular weight, and the polydispersity of the fractions and of the unfractionated LLDPE B. The results clearly confirm the existence of a huge intermolecular heterogeneity in the LLDPE B sample and also reveal a correlation between the average short-chain branching content and the average molecular weight of the fractions: The lower the branching content, the higher the average molecular weight.

Table III Onset Temperature of Crystallization, High- and Low-Temperature Peak of Crystallization, Onset Temperature of Melting, Peak Temperature of Melting, and Degree of Crystallinity χ_c of the Fractions and LLDPE B

Sample	Onset Cryst. (°C)	Cryst. Peak 1 (°C)	Cryst. Peak 2 (°C)	Onset Melting (°C)	Melting Peak (°C)	χ_c (%)
LLDPE B	114	111	—	120	127	42
B5	121	117	86	123	133	56
B4	113	110	72	122	129	50
B3	103	98	64	104	114	43
B2	96	90	54	96	108	36
B1	90	82	45	85	94	32
B0	77	58	—	33	61	10

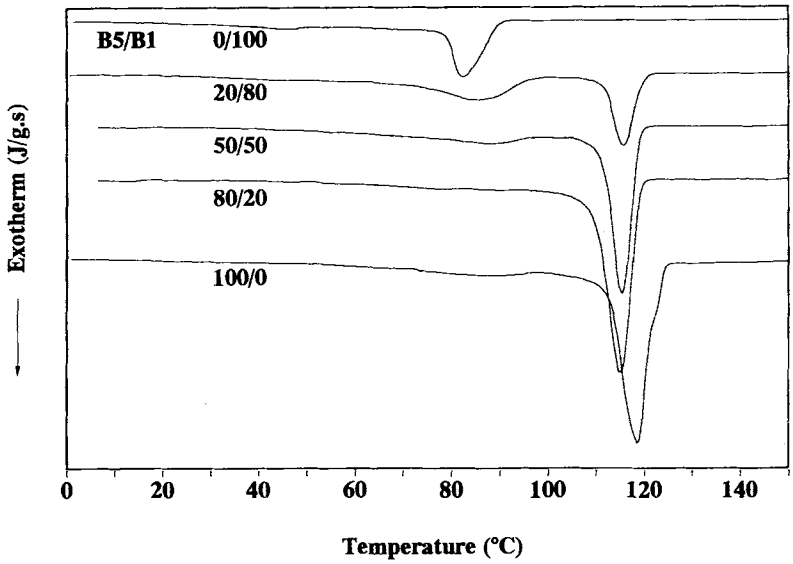

Figure 2 Crystallization exotherms of the B5/B1 blends.

Thermal Behavior

Figure 1 shows the crystallization exotherms of the fractions and LLDPE B. Increasing the short-chain branching content results in a decrease of the onset temperature of crystallization from the melt and in smaller exotherms. The fractions exhibit a first large crystallization exotherm and a second smaller exotherm about 35°C lower in temperature (Table III). This double-crystallization behavior has already been reported for SCB fractions of LLDPE[5,7]; its origin has, however, not been revealed. The crystallization exotherms of the blends are given in Figure 2. For the blends 20/80 and 50/50, a high-temperature peak (HTP) corresponding to the formation of thick lamellae and a low temperature peak (LTP) due to secondary crystallization of thinner lamellae can be detected. The low-temperature peak is not clearly distinguishable in the exotherm of blend 80/20.

The peak temperature of the first exotherm (HTP) is decreased in the blends by 2°C compared to fraction B5 (Table IV). This depression is caused by the increased entropy by introducing fraction B1. The crystalline lamellae formed during the first exotherm (HTP) are acting as nuclei in the secondary crystallization. As a result, the second exotherm (LTP) shifts to higher temperatures as the B5 content in the blend increases. The decrease of the peak temperature of the highest exotherm (HTP) and the increase of the peak temperature of the lowest exotherm (LTP) compared to the pure components clearly illustrate the mutual influence of both components during crystallization. Nevertheless, both fractions crystallize to a large extent into separate lamellae as shown by the double-crystallization behavior.

The melting endotherms of the different fractions and of LLDPE B are represented in Figure 3. An increase of the SCB content gives rise to a shift of the melting endotherms to lower temperatures (Table III). The peak and end melting temperature of fractions B5 and B4 are higher than those of unfractionated LLDPE B. Cocrystallization of the weakly branched molecules with molecules having a slightly higher branching degree in the unfractionated copolymer LLDPE B can be the reason for the lower melting peak.

The melting endotherms of the B5/B1 blends are plotted in Figure 4. The 20/80 and 50/50 blends clearly exhibit a double melting peak, corresponding

Table IV High- (HTP) and Low-Temperature Peak (LTP) of Crystallization (*C*), High- and Low-Temperature of Melting (*M*), Degree of Crystallinity (χ_c) for the Blends of Fractions B5 and B1

Sample (B5/B1)	HTP *C* (°C)	LTP *C* (°C)	HTP *M* (°C)	LTP *M* (°C)	χ_c *M* (%)
100/0	117	—	133	—	56
80/20	115	—	130	—	58
50/50	115	88	127	94	46
20/80	115	84	127	93	36
0/100	—	82	—	94	32

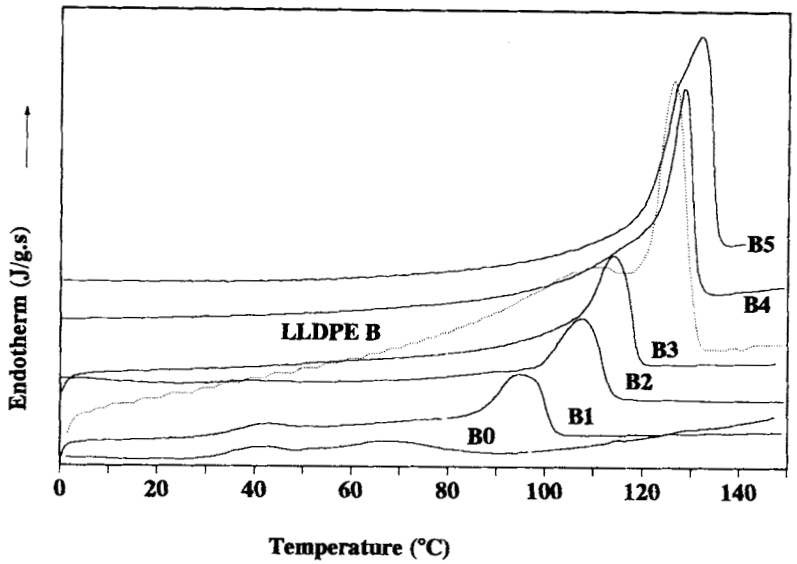

Figure 3 Melting endotherms of the fractions and LLDPE B.

to two populations of lamellae, formed by the components. For the blend 80/20, only one broad melting peak can be detected. The melting peak temperatures of the blends are depressed compared to the B5 fraction (Table IV).

The crystallinity of the fractions studied decreases from more than 50% to about 10% with increasing SCB content (Table III). The total crystallinity of the blends follows the rule of mixtures within the experimental error (Fig. 5).

Morphology

Spherulitic Texture

During crystallization from the melt, all the fractions exhibit the typical light-scattering pattern of spherulites. The intensity of the SALLS pattern, which depends on the number and volume of the spherulites, and thus on the total amount of crystallized material, strongly increases at the onset temperature of crystallization and levels off at much lower tem-

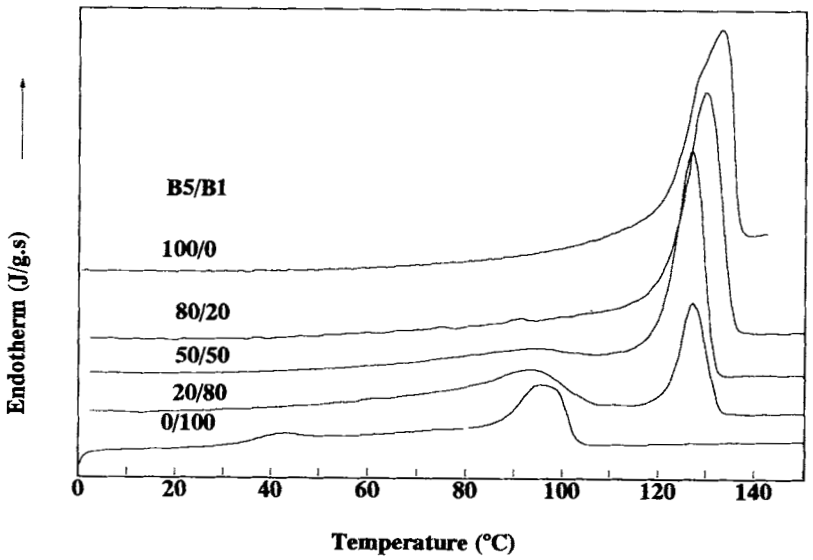

Figure 4 Melting endotherms of the B5/B1 blends. The fractions B1 and B5 are added as melting-point references.

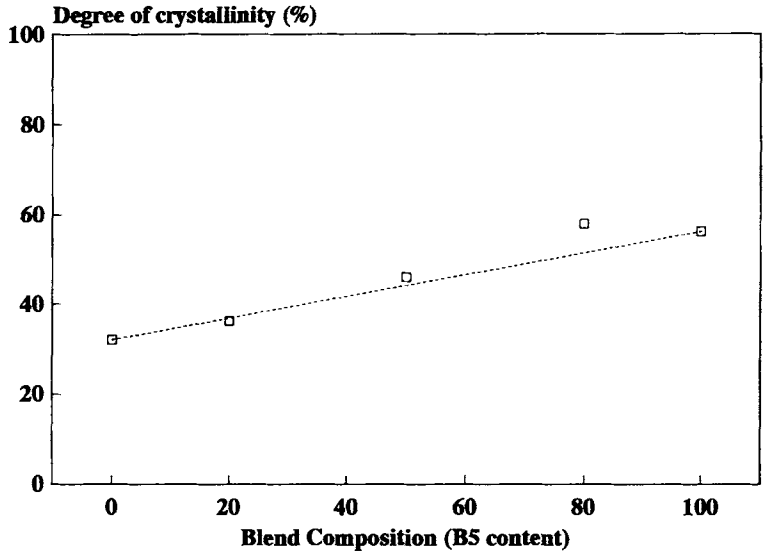

Figure 5 Degree of crystallinity of the B5/B1 blends as a function of the blend composition.

peratures (Fig. 6). The stepwise increase of the SALLS intensity of B5/B1 blends 20/80 and 50/50 (Fig. 7) results from the separate crystallization of both fractions. The onset of the second step in the crystallization process of the blends is shifted toward higher temperatures compared to fraction B1. This is the result of the nucleation effect of the crystalline phase of fraction B5 on the crystallization behavior of fraction B1. For the blend 80/20, a singular increase of the SALLS intensity is detected, which is, however, spread over a broader temperature range than for fraction B5.

The average spherulitic radius of the fractions decreases with increasing short-chain branching content. The average radius of the spherulites formed in the blends is compared with that of the

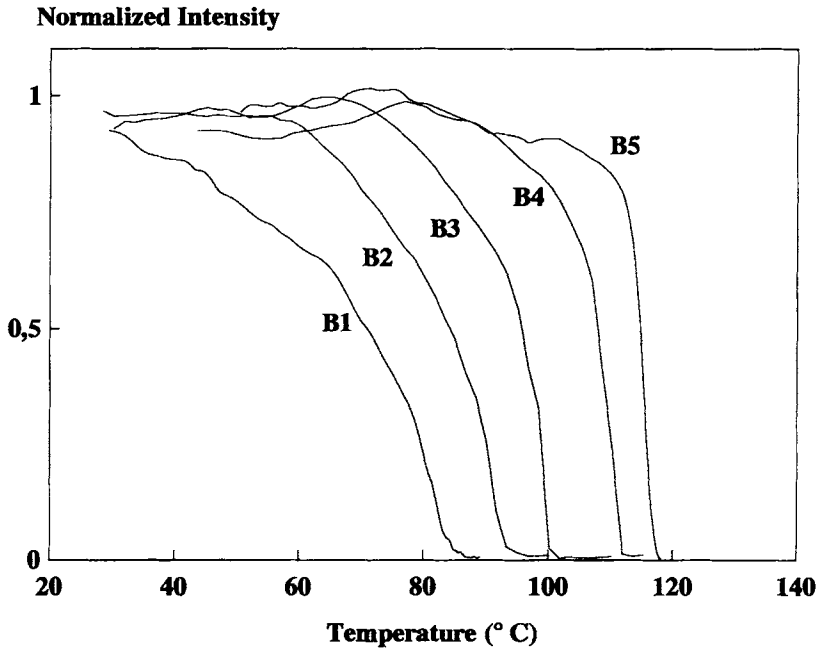

Figure 6 Hv Salls intensity of the fractions and LLDPE B as a function of the temperature during crystallization from the melt.

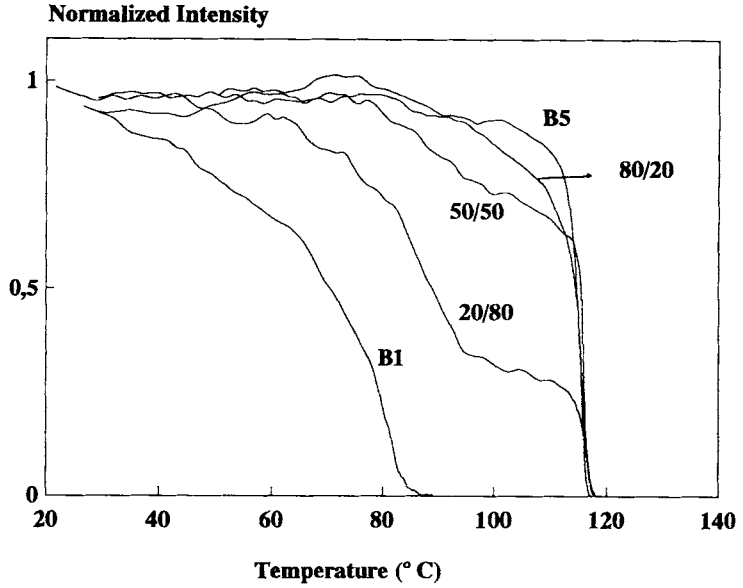

Figure 7 Hv Salls intensity of the B5/B1 blends as a function of the temperature during crystallization from the melt.

fractions in Figure 8. In the case of the blends, the average SCB content has been calculated using the average SCB contents of the fractions and their weight percent in the blend. Although the crystallization process of each blend is controlled by fraction B5, the spherulitic morphologies are different. The higher the content of fraction B1 in the blends, the lower the average spherulitic radius. The blend with 20% B5 and 80% B1 does not exhibit the typical spherulitic scattering pattern. The morphology of the blends does not only depend on the first crystallizing component, but is also strongly influenced by the segregated component.

Lamellar Semicrystalline Morphology

From SAXS measurements of the fractions, it has been observed that the maximum of the Lorentz-corrected intensity curves shifts to higher scattering

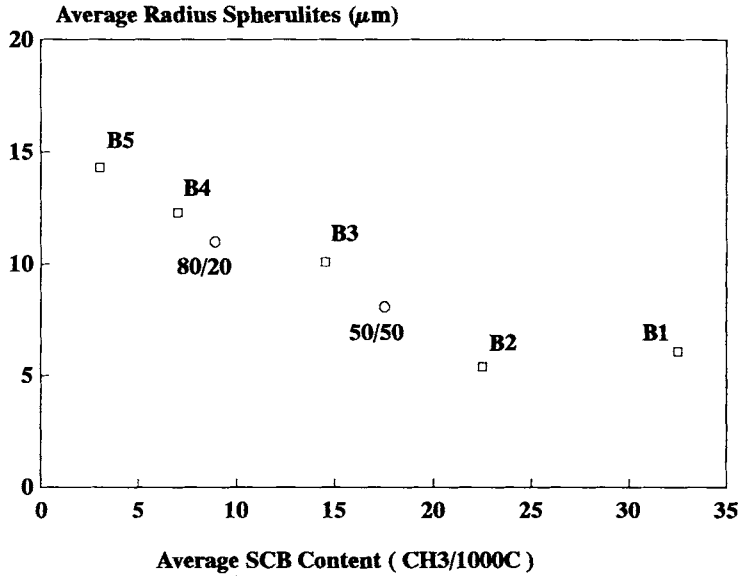

Figure 8 Average radius of the spherulites of the fractions and the blends as a function of the short-chain branching content.

angles and becomes broader as the branching content increases. The Lorentz-corrected SAXS patterns of the blends exhibit only one peak, which is still broader and less symmetric. The periodicity L can be calculated by applying Bragg's law to the scattering maximum of the Lorentz-corrected intensity. The periodicity L calculated for the fractions and the blends are plotted in Figure 9 as a function of the average short-chain branching content. An increase of the SCB content leads to a decrease of the average lamellar periodicity of the fractions and of the blends as well. The presence of only one scattering maximum in the diffractograms of the blends, while the DSC thermograms clearly show two different crystal populations, indicated that the segregated component crystallizes in between the lamellae of fraction B5.

The average lamellar thickness C_1 is repeatedly calculated using the relation $C_1 = L \cdot \phi$, where ϕ is the volume crystallinity of the sample. Though this is a fast and easy method, parallel lamellae are assumed and the lamellar thickness is frequently overestimated compared to more reliable methods of calculation.[29] The blends exhibit one broad scattering maximum, from which one value of the periodicity can be calculated. As a consequence, only a single value for the crystalline lamellar thickness can be deduced. The DSC and SALLS crystallization data, however, indicated that both fractions B1 and B5 within the blends were crystallizing into separate lamellar populations of different average thickness. These results clearly illustrate that one has to be very careful in calculating the lamellar thickness using the periodicity. In the case that the real semicrystalline morphology is much more complicated than is the simple two-phase model, SAXS measurements should be combined with other techniques (e.g., TEM) to reveal the lamellar structure. This has been recognized by Voigt-Martin and Mandelkern.[30]

The calculated correlation function $\gamma_1(r)$ can yield more detailed information about the formation of lamellar stacks in the samples. If the lamellae are packed into well-formed stacks and the crystalline thickness distribution is narrow, the correlation function will reach a high maximum after the self-correlation zone.[30] Low values of the first maximum are the result of distorted lamellar packing and/or broad lamellar thickness distributions. For the fractions, the maximum is higher when the SCB content increases (Fig. 10). Normally, one would expect that an increase of the branching content would result in a more distorted morphology.[18,19,31] The concomitant decrease of the molecular weight, however, influences the morphology in the reversed way.[12,13,31] These observations were also confirmed in a recent TEM study[9] on narrow PTREF fractions. The maximum of the correlation function of the blends is strongly decreased as compared to the fractions. The DSC and SALLS experiments demonstrated the presence of two distinct lamellar populations in the blends. This results in a much broader lamellar thickness distribution and must be considered as the reason for these low correlation values.

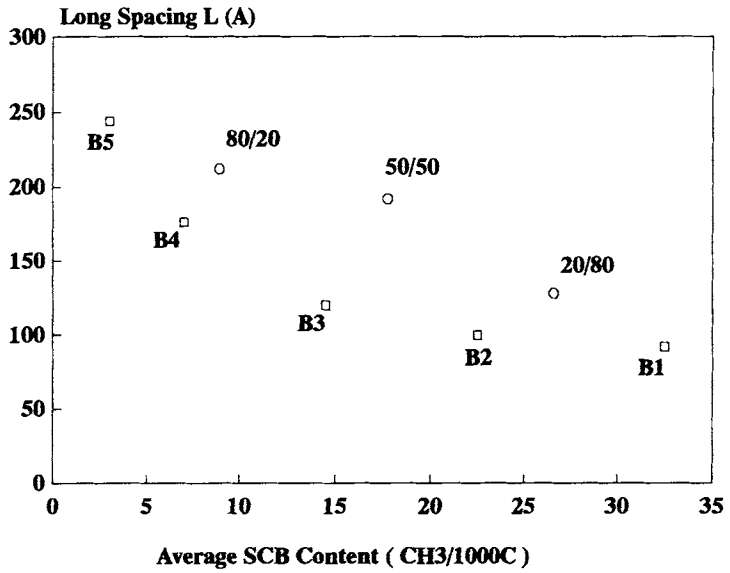

Figure 9 Average periodicity L of the fractions and the blends as a function of the short-chain branching content.

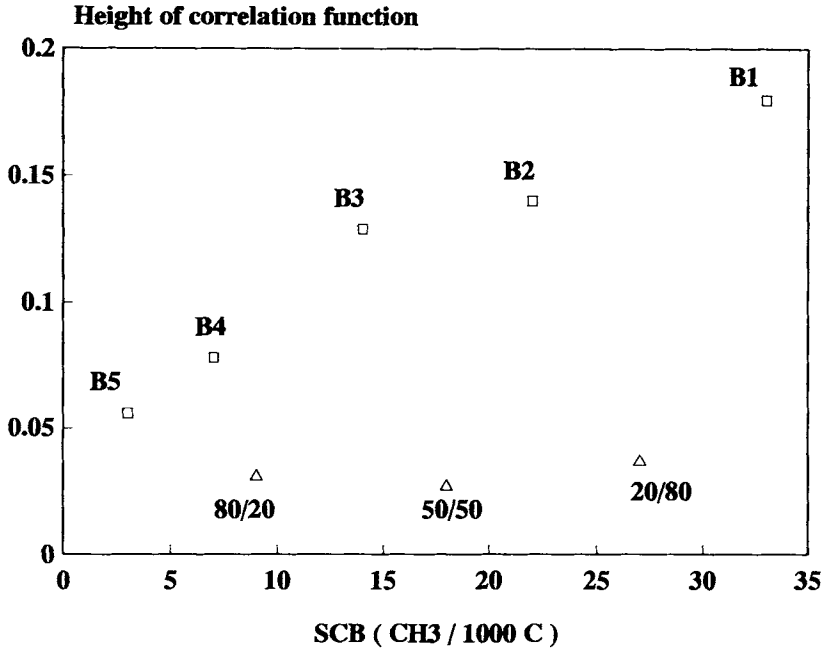

Figure 10 Height of the first maximum of the correlation function of the fractions and the blends.

CONCLUSIONS

The average short-chain branching content is strongly influencing the thermal behavior of PTREF fractions of 1-octene LLDPE: the end melting point, onset temperature of crystallization, and degree of crystallinity decrease with increasing SCB content. A higher SCB content results in a smaller average radius of the spherulites. The periodicity L of the fractions strongly decreases with increasing SCB content.

The concomitant decrease of the molecular weight with increasing short-chain branching content of the fractions causes a lower distortion of the lamellar morphology, in spite of the distorting effect of the side branches.

In the unfractionated LLDPE B, characterized by a very broad comonomer distribution, some degree of cocrystallization takes place resulting in a melting-point depression.

There is clear evidence that in the blends of the fractions having the lowest and the highest branching content the fractions crystallize into two different lamellar populations, although they exhibit a mutual influence. DSC and SALLS experiments have demonstrated that the crystalline phase of fraction B5 exerts a nucleation effect on the crystallization behavior of fraction B1. Both fractions determine the spherulitic morphology in a cooperative way.

The authors (F. D. and G. G.) are indebted to the Belgian National Science Foundation NFWO for financial support given to the MSC Laboratory.

REFERENCES

1. S. Hosoda, *Polym. J.*, **20**(5), 383 (1988).
2. L. Wild, T. Ryle, and D. Knobeloch, *Polymer Preprints*, **23**(2), 133 (1982).
3. E. Kelusky, C. Elston, and R. Murray, *Polym. Eng. Sci.*, **27**(20), 1562, (1987).
4. P. Schouterden, G. Groeninckx, B. Van der Heijden, and F. Jansen, *Polymer*, **28**, 2099 (1987).
5. D. Wilfong and G. W. Knight, *J. Polym. Sci. Polym. Phys. Ed.*, **28**, 861 (1990).
6. H. Springer, A. Hense, and G. Hinrichsen, *J. Appl. Polym. Sci.*, **40**, 2173 (1990).
7. F. Defoor, G. Groeninckx, P. Schouterden, and B. Van der Heijden, *Polymer*, to appear.
8. P. Schouterden, M. Vandermarliere, C. Riekel, M. Koch, G. Groeninckx, and H. Reynaers, *Macromolecules*, **22**, 237 (1989).
9. F. Defoor, G. Groeninckx, P. Schouterden, and B. Van der Heijden, *Polymer*, to appear.
10. F. Defoor, G. Groeninckx, H. Reynaers, P. Schouterden, and B. Van der Heijden, to appear.

11. I. G. Voigt-Martin and L. Mandelkern, *J. Polym. Sci. Polym. Phys. Ed.*, **19,** 1769–1790 (1981).
12. I. G. Voigt-Martin, E. W. Fischer, and L. Mandelkern, *J. Polym. Sci. Polym. Phys. Ed.*, **18,** 2347 (1980).
13. I. G. Voigt-Martin and L. Mandelkern, *J. Polym. Sci. Polym. Phys. Ed.*, **22,** 1901 (1984).
14. G. M. Stack, L. Mandelkern, and I. G. Voigt-Martin, *Macromolecules,* **17,** 321 (1984).
15. M. Glotin and L. Mandelkern, *Colloid Polym. Sci.,* **260,** 182 (1982).
16. G. Chiu, R. G. Alamo, and L. Mandelkern, *J. Polym. Sci. Polym. Phys. Ed.*, **28,** 1207 (1990).
17. L. Mandelkern and J. Maxfield, *J. Polym. Sci. Polym. Phys. Ed.*, **17,** 1913 (1979).
18. S. Hosoda, K. Kojima, and M. Furuta, *Makromol. Chem.*, **187,** 1501 (1986).
19. I. G. Voigt-Martin, R. Alamo, and L. Mandelkern, *J. Polym. Sci. Polym. Phys. Ed.*, **24,** 1283 (1986).
20. S. Hu, T. Kyu, and R. Stein, *J. Polym. Sci. Polym. Phys. Ed.*, **25,** 71 (1987).
21. T. Kyu and R. Stein, *J. Polym. Sci. Polym. Phys. Ed.*, **25,** 89 (1987).
22. R. G. Alamo, R. H. Glaser, and L. Mandelkern, *J. Polym. Sci. Polym. Phys. Ed.*, **26,** 2169 (1988).
23. M. T. Braña, J. I. Sainz, B. Terselius, and U. W. Gedde, *Polymer,* **30,** 410 (1989).
24. A. Gustafsson, M. T. Braña, and U. W. Gedde, *Polymer,* **32,** 426 (1991).
25. D. R. Norton and A. Keller, *J. Mater. Sci.,* **19,** 447 (1984).
26. L. Wild, T. R. Ryle, D. C. Knobeloch, and I. R. Peat, *J. Polym. Sci. Polym. Phys. Ed.*, **20,** 441 (1982).
27. S. Nakano and Y. Goto, *J. Appl. Polym. Sci.*, **26,** 4217 (1981).
28. G. Kortleve and C. G. Vonk, *Kolloid Polym.*, **225,** 124 (1968).
29. C. G. Vonk, *Makromol. Chem. Macromol. Symp.*, **15,** 215 (1988).
30. I. G. Voigt-Martin and L. Mandelkern, *J. Polym. Sci. Polym. Phys. Ed.*, **27,** 967 (1989).
31. L. Mandelkern, *Polym. J.*, **17,** 337 (1985).

Received February 18, 1992
Accepted May 27, 1992